

vative or minimally invasive methods for glucose monitoring. Detecting diabetes remains difficult since finger-pricking procedures are slightly painful and costly to the users [3]. Therefore, apparent demand for a non-invasive pain-free biosensor for glucose monitoring is established [4,5].

Microwave sensing techniques are emergent for non-invasive dielectric measurements as they can provide information on biological tissues without or with minimal contact with the medium. In addition, microwaves can overcome structural obstacles and permeate biological tissues without any health risks to the operator or the subject [6].

This paper proposes a planar sensor operating in the centimetre-wave band at 2.3 GHz for non-invasive measurements of blood glucose levels. The sensor is fabricated using four similar hexagonal-shaped complementary split-ring resonators engraved in the ground plane of a microstrip line, organised as a honey-cell structure. The sensor sensitivity is enough to measure glucose samples at the level of interest compared to a single complementary split-ring resonator (CSRR) due to the honey-cell configuration. The proposed honey-cell CSRR has a steep resonance response of about -50 dB than the conventional CSRR of low depth (-20 dB) [7]. Testing lossy tissues would dampen the induced resonance; therefore, robust resonances would help acquire a better resolution and sensitivity. Modelling and 3D electromagnetic simulations of the microwave sensor with a human fingertip (inserted in the sensing region) are presented and compared to preliminary measurements. The influence of the different finger layers thicknesses on the microwave sensor was also assessed. This study aims to measure the changes in frequency due to the variations in glucose level by placing the finger on the resonator.

2. Materials and methods

2.1. Resonant method for glucose sensing

Various characterisation approaches have been developed to study the interaction of microwaves with the matter. These techniques can be classified into three categories: free-space, transmission line, and resonant method [6]. This last technique is distinguished for its high accuracy. It is based on the change of the resonant sensor characteristics (resonant frequency, bandwidth and quality factor) when a dielectric material is applied on its surface, resulting from the interaction of the material with the electromagnetic field. The complex relative permittivity $\epsilon_r = \epsilon'_r - j\epsilon''_r$ describes this interaction between the electromagnetic field and the biological tissue, where ϵ'_r is the dielectric constant, representing the tissue's ability to store electrical energy and ϵ''_r is related to the losses associated with the dissipation of electromagnetic energy in the tissues.

The result of the interaction of the material with the electromagnetic field is represented through the transmission response of the resonator in Fig. 1.

2.2. Honey-cell CSRR sensor design

To obtain a miniaturised sensor, we focused on CSRRs with the same structure as split-ring resonators SRRs since both have a band-stop filter behaviour; however, CSRRs are engraved in a metal layer. Several shapes (square, circular ...) could be considered in CSRR resonators design [8,9]. Instead of selecting a conventional shape, we exerted a single hexagonal cell to perform an array of CSRRs efficiently. Indeed, those cells can be fitted together; thus, a honey-cell form can be well adapted.

In this study, the honey-cell CSRR's structure was chosen due to its capacity to obtain better sensitivity. In-vitro measurements of aqueous glucose solutions have already been performed with this

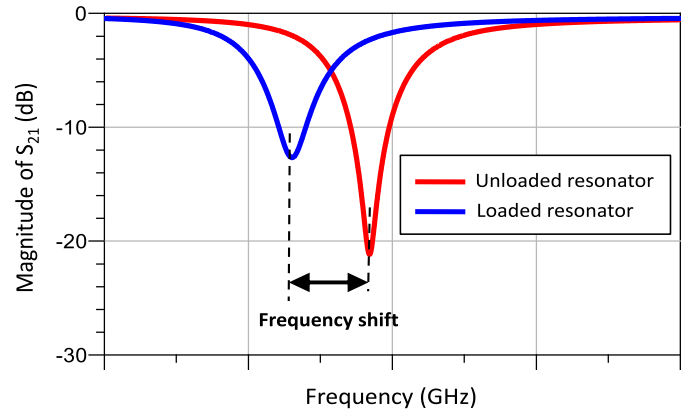


Fig. 1. The transmission coefficient response of the resonator loaded and unloaded.

type of sensor. These solutions mimicked the blood at relevant diabetes Type two glucose concentrations (70–120 mg/dl) [7,10]. The design on a classical standard substrate was optimised using numerical simulations to operate at a particular frequency with a good level of sensitivity for variations in glucose dielectric properties. The reference [8] mentioned above discussed the effect of all these design parameters in the detection performance of the CSRRs.

The sensor used consisted of four similar hexagonal resonators arranged in a honey-cell structure, as shown in Fig. 2 (a). Two single CSRRs are placed horizontally along the transmission feed line with centre-to-centre distance; $C = 13$ mm, the two other cells are placed vertically with the same distance. The sensor was designed on an FR4 substrate (with dielectric constant $\epsilon'_r = 4.6$, loss tangent $\tan\delta = 0.02$ and thickness $h = 0.73$ mm); the overall dimensions of the substrate are $L = 40$ mm and $W = 30$ mm. The hexagonal unit-cell includes two concentric split-rings etched in the copper ground plane. The outer ring of the unit-cell was designed with a diagonal length of $a = 9.8$ mm, a side width $s = 0.4$ mm and a split gap $g = 0.4$ mm.

The inner ring was designed with a similar side width and split gap to the outer one, nevertheless with a diagonal length of $b = 7.5$ mm. The inter distance between the two rings which control the coupling was at $t = 0.4$ mm. These dimensions were optimised with the ANSYS HFSS software to obtain an unloaded resonance frequency around 2.3 GHz. All the geometrical parameters of the honey-cell CSRR sensor are indicated in the legend of Fig. 2. The feed-line of the structure is a 50Ω microstrip line whose width was optimised to $W_1 = 1.42$ mm. This copper line was realised on the upper face of the FR4 dielectric substrate with a length of $L = 40$ mm. Each end of the access-line on the upper surface of the structure was soldered to a 50Ω SMA coaxial connector to perform S-parameter measurements, as shown in Fig. 2 (b) and (c).

2.3. Simplified human finger model

A simplified model was implanted in ANSYS HFSS to mimic a human index finger, considering the average thickness and permittivity of the layers composing the finger. Typically, the skin in the finger is composed of three layers: the epidermis, the dermis and the hypodermis. Connective tissues, hair follicles and sweat glands are found in the dermis layer, while subcutaneous fat usually fills the hypodermis [11,12].

Subungual arterial arcades and dorsal digital veins are located beneath the hypodermis [12] in addition to the distal phalanx, which is a flat rough bone that supports the finger pulp (Fig. 3(a)). Based on the anatomy of the human finger, a simplified model including four layers of biological tissues was therefore developed. The finger is modelled by a layer of skin followed by fat, blood,

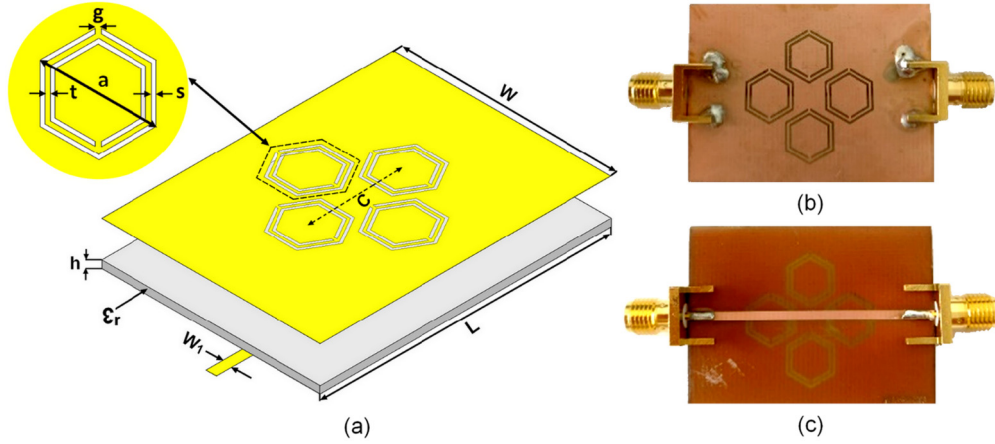


Fig. 2. 3D configuration of the honey-cell CSRR in (a), and the fabricated prototype of the CSRR sensor: (b) Ground plane and (c) Microstrip line. Here are the values in millimetres of different parameters for CSRR design in Fig. 2.a: $g = 0.4$; $t = 0.4$; $s = 0.4$; $a = 9.8$; $c = 13$.

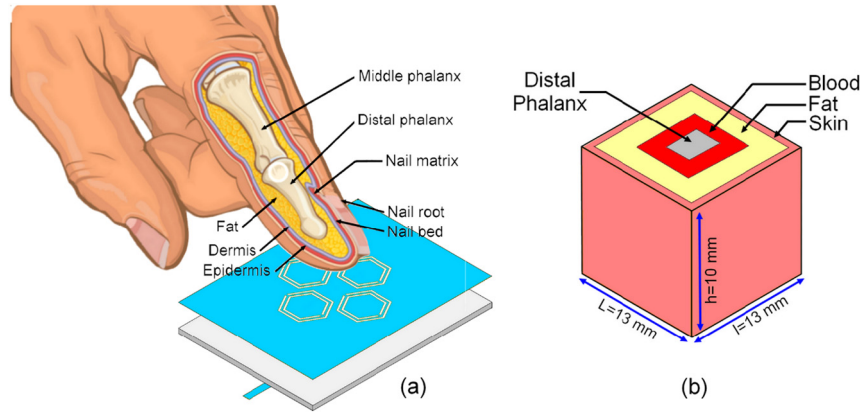


Fig. 3. Anatomy of a finger in (a) and the simplified finger model in (b).

and finally, the rectangular bone. The simplified model is shown in Fig. 3b. The dielectric parameters values of each tissue at 2.4 GHz composing the finger model [13] are detailed in Table 1 below.

The modelled finger length (h) under HFSS is of the order of 10 mm. The dimensions of the finger (13 mm x 13 mm) were chosen so that the finger, once placed on the sensor, covers the entire sensitive area of the sensor representing the middle part of the CSRR [14]. These dimensions correspond to those of an average female adult human finger and, more precisely, the index. The finger placement in the sensing region is also illustrated in Fig. 3(a) for blood glucose monitoring.

3. Results

Using HFSS, the 4-layer finger model was placed on top of the sensor to investigate the resonant frequency and magnitude changes.

Table 1
Dielectric parameters of finger layers @ 2.4 GHz [13].

Tissue	Thickness (mm)	Dielectric constant
Skin	0.5	35
Fat	0.5	5.5
Trabecular blood	2.5	59
Bone	4	20

3.1. Unloaded honey-cell CSRR sensor responses

Fig. 4 compares the hexagonal cell's simulation and measurement results with the honey-cell CSRR sensor from 1 to 4 GHz without the finger. The measured resonant frequencies are 2.36 GHz and 2.376 GHz, respectively, for the single hexagonal and honey-cell CSRR circuits.

As expected, a great agreement was obtained between the measurements and the predicted numerical simulations. A minimal frequency shift is observed between experimental and simulated resonant frequency: 20 MHz for the hexagonal-unit cell and 35 MHz for the honey-cell. These differences are attributed to the etching precision while designing the sensor. In addition to the inaccuracy of the dielectric constant value of the FR4 substrate in the considered frequency band. The advantage of the honey-cell structure compared to the single hexagonal one is that the quality factor increased, leading to a steeper resonance peak. Hence, a higher sensitivity on blood glucose detection is anticipated.

3.2. Loaded honey-cell CSRR sensor responses and pressure effect

Fingertip simulation revealed that filling the sensor with a human finger lead to a reduction in the resonant frequency of about 380 MHz as shown in Fig. 5.

The proposed honey-cell circuit has been tested through a simple in-vivo test by placing the index finger perpendicularly on the top of the sensor, which represents an intuitive and reproducible position (Fig. 3). The subject was a 23 years-old healthy female. The tests were performed while the subject was in a fasting state

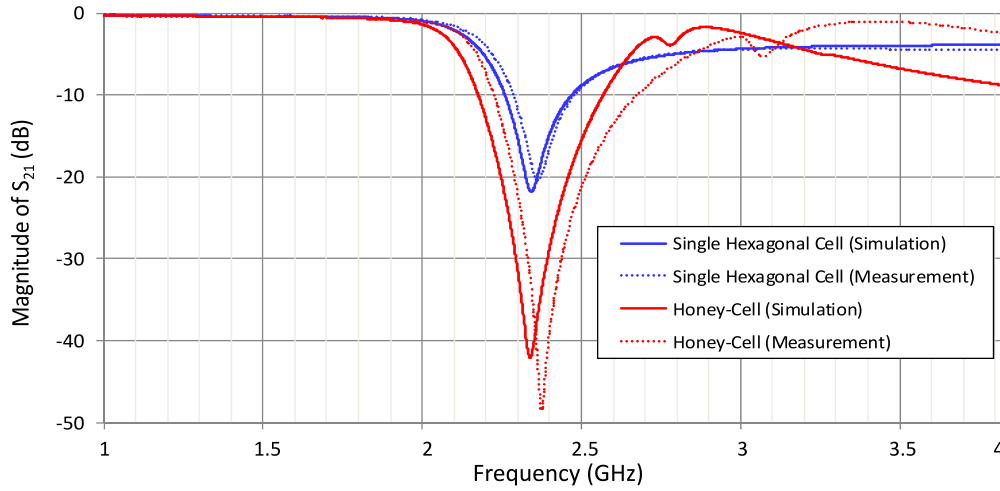


Fig. 4. Comparison between simulated and measured transmission coefficient (S_{21}) of unloaded sensors.

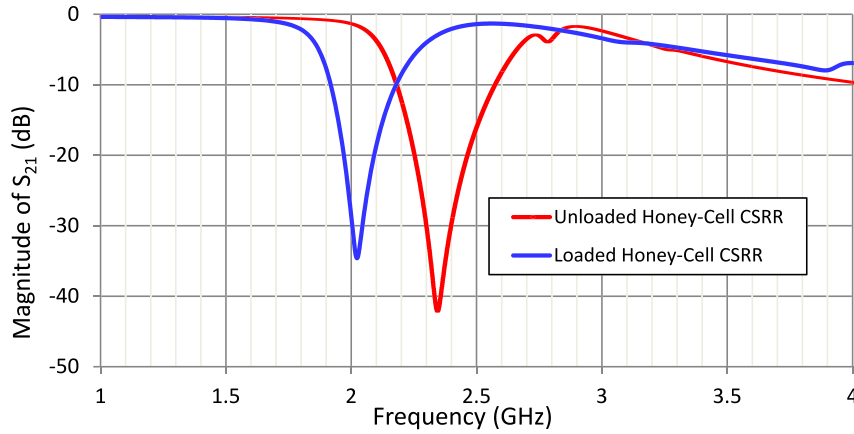


Fig. 5. Simulations of transmission coefficients (S_{21}) of the Honey Cell sensor unloaded and loaded with the finger on the top.

to ensure low glucose levels. To validate the finger model by placing the index perpendicularly on the top of the sensor and applying various pressure levels. Fig. 6 represents several measurements of the magnitude of the transmission coefficient S_{21} obtained after applying more or less firmly the finger on the surface of the sensor. This pressure effect on the sensor modifies the frequency shift and the notch level of the resonant sensor. It is noticed that between low and medium pressure, the amplitude difference of S_{21} is about 30 dB. The application of a medium pressure shifts the resonant frequency from 80 to 120 MHz towards the low frequencies compared to the case of low pressure. The low pressure is performed by just putting the finger in contact and on top of the sensor without applying any pressure.

When applying a medium pressure of the finger, the measured resonant frequency shifted towards low frequencies by 230 MHz while the simulation shows a frequency shift of 380 MHz (Fig. 7).

Many thickness variations could be potentially studied to assess the effect of the applied pressure. Therefore, simulations while varying the thicknesses of the skin, fat and blood layers in contact with the sensor (each layer separately) were performed to examine the effect of each layer. Accordingly, only the superficial sides of the layers vary to mimic a diminution of superficies in the surrounding areas. The skin and fat layers vary from 0 to 0.5 mm and the blood from 0 to 2.5 mm, as shown in Figs. 8(a) and (b). A correlation was found between the thickness of the layers and the frequency shift Δf . The thickness increases, the Δf increases lin-

early in the skin layer. However Δf increases quadratically in the fat and capillary blood layers as the thickness increases.

Moreover, it was observed that the variation of the skin layer thickness influences the resonant frequency more than the other tissues. A shift in the frequency of 110 MHz due to skin layer changes has occurred as compared to 9 MHz for the fat layer and 4.2 MHz for the blood one (while decreasing the layer by 100%) (Fig. 8.b).

Simulations of the transmission parameter, considering that the hypodermis containing capillary blood vessels is being flattened, hence reducing its thickness, are shown in Fig. 9. Furthermore, there were considerable shifts in the resonant frequency and steeper resonance depths while varying the thickness of the blood (h_{Blood}).

By comparing simulated and measured results of the loaded sensor, the best-suited configurations were the ones with relatively thin layers of skin, fat and a thicker layer of blood. While decreasing the thickness of the skin, fat and the blood by 10%, 10% and 20%, respectively ($h_{\text{Skin}} = 0.45$ mm $h_{\text{Fat}} = 0.45$ mm and $h_{\text{Blood}} = 2$ mm), a frequency shift of 100 MHz is observed compared to the measured response.

Then while decreasing the thickness of these layers by 50, 40% and 50%, respectively ($h_{\text{Skin}} = 0.25$ mm $h_{\text{Fat}} = 0.3$ mm and $h_{\text{Blood}} = 1.25$ mm), the frequency shift simulated was almost equal to the measured one.

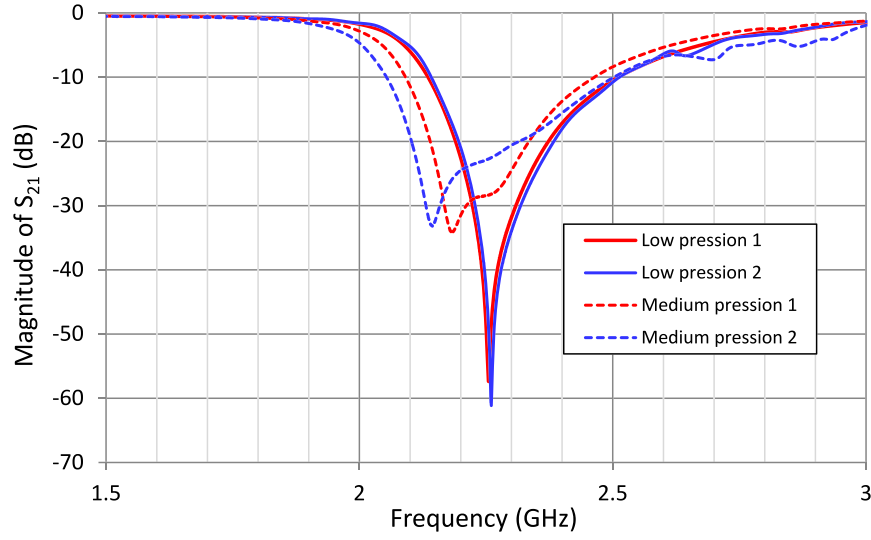


Fig. 6. Several measurements of the transmission coefficient (S_{21}) of the finger index placed on the top of the Honey-Cell CSRR with different pressures.

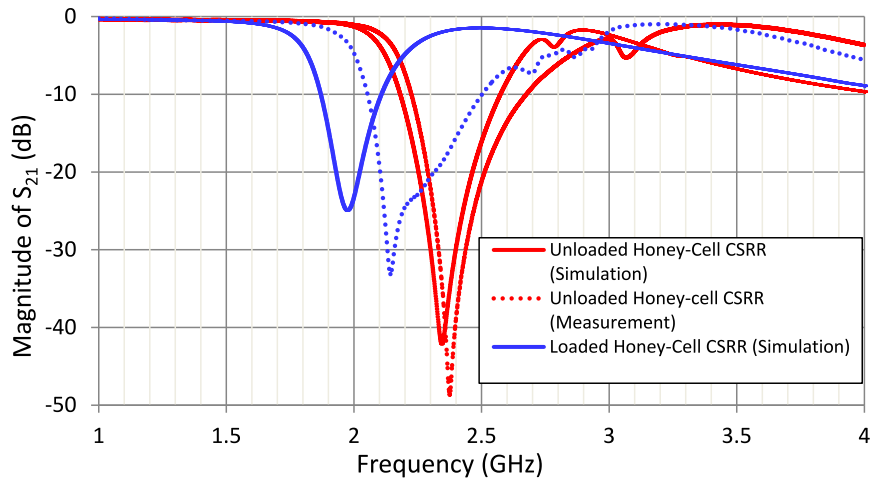


Fig. 7. Measurements and simulations of transmission coefficients (S_{21}) of the Honey Cell sensor loaded with the finger on its top by applying a medium pressure.

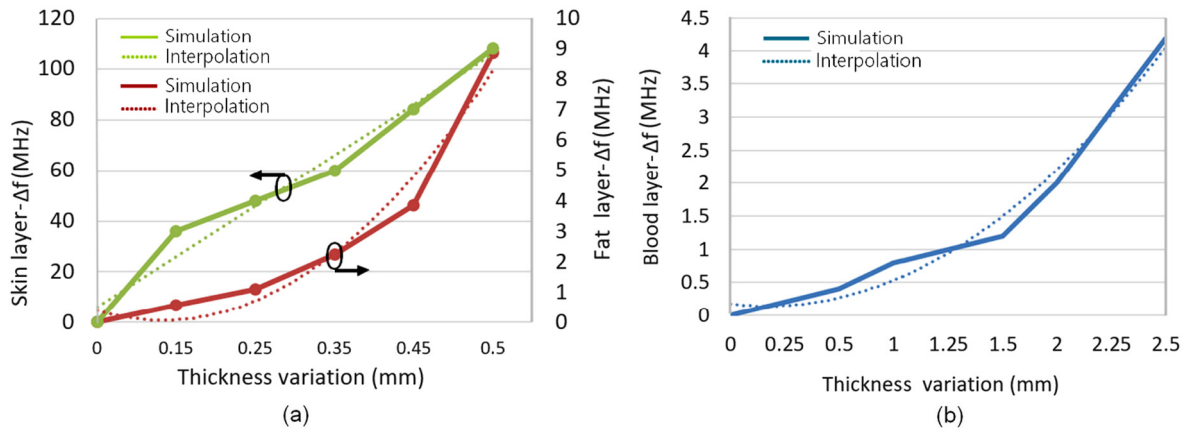


Fig. 8. Simulations of the transmission coefficient (S_{21}) of the Honey-Cell sensor loaded with the finger on the top while varying the thickness of the three layer (skin, fat and blood).

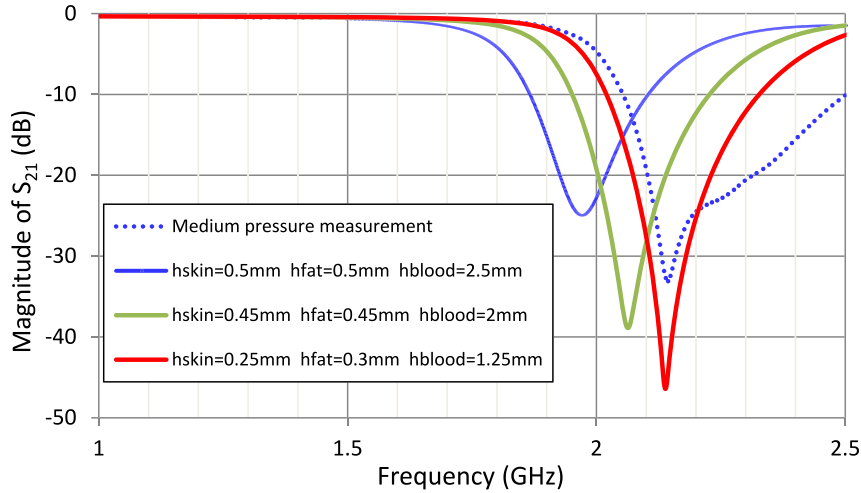


Fig. 9. Simulations of the transmission coefficient (S_{21}) of the Honey-Cell sensor loaded with the finger on the top while varying the thickness of the three layers (skin, fat and blood).

4. Discussion

These preliminary results of in-vivo experiments in order to measure the glucose amount in the blood of a person using the microwave sensor show that the experimental conditions must be more drastic than those of ex-vivo measurements done on calibrated liquids [10,13]. The measurements indicated that the finger as a superstrate could be very dynamic compared to the static simulated model. It was noticed that the measured resonant frequency, when a medium pressure of the finger, which is slightly higher than the low pressure of just putting the finger on the resonator, was applied on top of the sensor, is 150 MHz higher than the resonant frequency obtained with the simulated model. Therefore, the equivalent permittivity of the modelled finger is higher than the real one.

Moreover, the higher the finger pressure, the more the resonance shifted towards low frequencies with a decreasing magnitude. This could be since skin tissue is thinner while compressed and/or even more capillary blood vessels appear nearer to the sensitive region on the CSRR sensor.

In light of the obtained results, when varying the finger layers thicknesses independently, it was observed that the change in the skin layer thickness influences the resonant frequency more than the other ones due to its proximity to the sensor sensitive area, and it has a high permittivity of $\epsilon_r = 38$.

Regarding Fig. 6, which represents a set of 3 measurements per pressure variation, a best-fitted protocol has to be employed to maintain constant pressure, such as using a tiny pressure sensor in the middle of the honey cell, which can operate at a few kHz.

The obtained results show that the sensor sensitivity to the pressure is a crucial parameter, and it should be considered for the following reasons:

- The coupling between the sensor and the fingertip varies depending on the applied pressure. The soft tissue layers' effective thickness changes depending on the applied pressure.
- The blood is pushed away from the fingertip proportional to the applied pressure, altering the number of capillary blood vessels present in the tissue.

There are also several physiological factors such as the variable composition of the blood, body temperature, humidity conditions [15] and methodological ones like the method of measurement that may have a significant influence on measured scattering parameters.

Therefore in order to increase the reliability of the microwave sensor measurements, it is necessary to introduce a control of the strength applied by the finger on the sensor surface; thus the experimental results can be compared with simulations of its multilayer structure.

An integrated pressure sensor [16–18] would help to correct the microwave sensor readings when extreme pressure is applied. The pressure reading could be used in a machine learning algorithm that is been trained with pressure dataset to adjust the blood glucose level accordingly. Or possibly, when the sensor indicates high pressure, a warning is sent to the user interface advising to place the finger more conveniently. Regressions models [19,20] could correlate the frequency shifts to their corresponding glucose levels. If variations are not linear, deep learning models [21] could map the generated raw data to the accurate blood sugar levels.

5. Conclusion

This paper demonstrates simulations and experimental results on a centimetre-wave sensor to detect non-invasively glucose level changes of diabetic patients, the developed sensor consisting of four honey-cell hexagonal-shaped CSRRs. Electromagnetic simulations using a simple finger model with the main tissue layers developed with HFSS are compared with measurements using a sensor prototype. The achieved results clearly show the impact of the applying pressure of the finger on the microwave sensor. Further investigations are in progress to obtain a good reproducibility of experimental results using a best-fitted pressure protocol to maintain the finger stable on top of the CSRR sensor and measure the glucose level precisely. In addition, tests by varying the finger's position horizontally instead of vertically are in progress to determine whether the position influences in vivo measurements.

Human and animal rights

The authors declare that the work described has been carried out in accordance with the Declaration of Helsinki of the World Medical Association revised in 2013 for experiments involving humans as well as in accordance with the EU Directive 2010/63/EU for animal experiments.

Funding

This work did not receive any grant from funding agencies in the public, commercial, or not-for-profit sectors.

Author contributions

All authors attest that they meet the current International Committee of Medical Journal Editors (ICMJE) criteria for Authorship.

CRedit authorship contribution statement

Karina Abdesselam: Initial draft preparation, Conceptualization, Methodology, Simulations, Measurements, Data interpretation.

Chaouki Hannachi: Simulations, Drafting the manuscript, Reviewing and editing.

Rania Shahbaz: Drafting the manuscript, Editing, Measurements assistance.

Frederique Deshours: Supervision, Drafting the manuscript, Figures revision.

Georges Alquié: Supervision, Drafting the manuscript.

Ala Omer: Technical advices, Reviewing.

Hamid Kokabi: Supervision and coordination, Final deep revising of the manuscript.

Jean-Michel Davaine: Medical advices.

Declaration of competing interest

The authors declare that they have no known competing financial or personal relationships that could be viewed as influencing the work reported in this paper.

Acknowledgement

The authors are very thankful to researchers at GeePs, Mr Ousama Mouda Azzem, for his useful advices and to Mr Yves Chatelon for all his technical assistances.

References

- [1] Huo X, Gao L, Guo L, et al. Risk of non-fatal cardiovascular diseases in early-onset versus late-onset type 2 diabetes in China: a cross-sectional study. *Lancet Diabetes Endocrinol* 2016;4(2):115–24.
- [2] Spegazzini J, et al. Spectroscopic approach for dynamic bioanalyte tracking with minimal concentration information. *Sci Rep* 2014;4:7013.
- [3] World Health Organization, <https://www.who.int/diabetes>.
- [4] Centers for Disease Control and Prevention. National Diabetes Statistics Report, 2020. Centers for Disease Control and Prevention. U.S. Dept. of Health and Human Services, Atlanta, GA, 2020.org.
- [5] Cunningham D, Stenken J. In vivo glucose sensing. Hoboken, N.J.: Wiley; 2010.
- [6] Chandra R, Zhou H, Balasingham I, Narayanan RM. On the opportunities and challenges in microwave medical sensing and imaging. *IEEE Trans Biomed Eng* July 2015;62(7):1667–982.
- [7] Omer AE, Shaker G, Safavi-Naeini S, Alquié G, Deshours F, Kokabi H, et al. Non-invasive real-time monitoring of glucose level using novel microwave biosensor based on triple-pole CSRR. *IEEE Trans Biomed Circuits Syst Dec*. 2020;14(6):1407–20.
- [8] Deshours F, Alquié G, Goudjil T, Kokabi H, Davaine J-M, Koskas F. Modélisation de résonateurs en anneaux fendus pour la mesure de permittivités complexes. In: *Colloque XXIèmes journées nationales microondes*; 2019. p. 14–7.
- [9] Al-Nuaimi Mustafa K Taher, Whittow Will. Compact microstrip band stop filter using SRR and CSRR: design, simulation and results; 2010. p. 1–5.
- [10] Omer AE, Shaker G, Safavi Naeini S, Kokabi H, Alquié G, Deshours F, et al. Low cost portable microwave sensor for non-invasive monitoring of blood glucose level: novel design utilising a four cell CSRR hexagonal configuration. *Sci Rep* 2020;10:15200. <https://doi.org/10.1038/s41598-020-72114-3>.
- [11] Gray Henry. *Anatomy of the human body*, USA, 1985.
- [12] The hypodermis. An Organ Revealed. L'Oréal. Retrieved 4 June 2013.
- [13] Gabriel C. Compilation of the dielectric properties of body tissues at RF and microwave frequencies, Report N.AL/OE-TR-1996-0037, Occupational and environmental health directorate, Radiofrequency Radiation Division, Brooks Air Force Base, Texas, USA, 1996.
- [14] Omer E, Shaker G, Safavi-Naeini S, Kokabi H, Alquié G, Deshours F. Compact honey-cell CSRR-based microwave newline biosensor for monitoring glucose levels. In: 2020 14th European conference on antennas and propagation (EuCAP); 2020. p. 1–5.
- [15] Vashist SK. Non-invasive glucose monitoring technology in diabetes management: a review. *Anal Chim Acta* 2012;750:16–27.
- [16] Hierold C, Clasbrummel B, Behrend D, Scheiter T, Steger M, Oppermann K, et al. Low power integrated pressure sensor system for medical applications 1999;73(1–2):58–67. [https://doi.org/10.1016/S0924-4247\(98\)00255-6](https://doi.org/10.1016/S0924-4247(98)00255-6).
- [17] Yamada K, Nishihara M, Kanzawa R, Kobayashi R. A piezoresistive integrated pressure sensor; 1983. p. 63–9.
- [18] Ishihara T, Suzuki K, Suwazono S, Hirata M, Tanigawa H. CMOS integrated silicon pressure sensor 1987;22(2):151–6. <https://doi.org/10.1109/jssc.1987.1052696>.
- [19] Gonzalez-Navarro F, Stilianova-Stoytcheva M, Renteria-Gutierrez L, Belanche-Muñoz L, Flores-Rios B, Ibarra-Esquer J. Glucose oxidase biosensor modeling and predictors optimization by machine learning methods. *Sensors* 2016;16(11):1483. <https://doi.org/10.3390/s16111483>.
- [20] Songlin Z, Lakshmi S, Jiachen Y, Xueping Z, Swee Ching T. Augmenting sensor performance with machine learning towards smart wearable sensing electronic systems, advanced intelligent systems. <https://doi.org/10.1002/aisy.202100194>.
- [21] Phan DT, Nguyen CH, Nguyen TDP, Tran LH, Park S, Choi J, et al. A flexible oh, wearable, and wireless biosensor patch with Internet of medical things applications. *Biosensors* 2022;12:139. <https://doi.org/10.3390/bios12030139>.